J. Fluid Mech. (2014), *vol.* 743, *pp* 32–59. © Cambridge University Press 2014
doi:10.1017/jfm.2013.682

Lattice Boltzmann approach to simulating a wetting–drying front in shallow flows

H. Liu[1],† and J. G. Zhou[2]

[1]Key Laboratory of Water and Sediment Sciences of Ministry of Education, School of Environment, Beijing Normal University, Beijing 100875, PR China

[2]School of Engineering, University of Liverpool, Brownlow Hill, Liverpool L69 3GQ, UK

(Received 22 September 2012; revised 30 June 2013; accepted 23 December 2013; first published online 3 March 2014)

The paper reports a new lattice Boltzmann approach to simulating wetting–drying processes in shallow-water flows. The scheme is developed based on the Chapman–Enskog analysis and the Taylor expansion, which is consistent with the theory of the lattice Boltzmann method. All the forces, such as bed slope and bed friction, are taken into account naturally in determining the wet–dry interface, without the use of either the spurious assumption of a thin water film on a dry bed or the non-physical extrapolation of certain variables such as water depth or velocity. This offers a simple and general model for simulating wetting–drying processes in complex flows involving external forces. Its verification is carried out by modelling several one-dimensional (1D) and two-dimensional (2D) flows: (i) 1D sloshing over a parabolic container; (ii) a 1D tidal wave over three adverse bed slopes; (iii) a 1D solitary wave run up on a plane sloping beach; (iv) a tsunami run up on a plane beach; (v) a 2D stationary case with wet–dry boundaries; (vi) a 2D long-wave resonance over a parabolic basin; and (vii) a 2D solitary wave run up on a conical island. The numerical results agree well with analytical solutions, other numerical results and experimental data, demonstrating the effectiveness and accuracy of the new approach.

Key words: computational methods, hydraulics, solitary waves

1. Introduction

Shallow-water flows are common phenomena in nature and exist in many engineering applications. Given the hydrostatic pressure nature and the negligible vertical acceleration, the nonlinear shallow-water (NLSW) equations can be obtained by integrating the Navier–Stokes equations over the water depth, which turns out to be a very powerful mathematical model for simulating long-wave hydrodynamics. In addition to conventional numerical methods, such as the finite volume method and the finite difference method for solving the NLSW equations, the lattice Boltzmann method (LBM) for simulating different complex flows has developed rapidly in recent decades. The LBM is based on a fully discrete kinematic model instead of a set of partial differential equations, and has several desirable properties, such as

† Email address for correspondence: haifei.liu@bnu.edu.cn

linear convection terms and nearest-neighbour stencils, leading to a simple model with parallel processes in coding. Using the LBM, the NLSW equations could be recovered in macroscopic scale, and it is suitable to investigate shallow-water problems. Since 1999, a number of researchers have carried out work on shallow-water problems using the LBM (Salmon 1999; Dellar 2002; Zhou 2002). The lattice Boltzmann shallow-water model was further developed by using multi-block mesh (Liu *et al.* 2010) and later the open boundary condition was improved (Liu *et al.* 2012).

A further common, important and natural phenomenon associated with shallow-water flows in river, coastal regions, etc., is wetting–drying processes in water flows such as wave run-up and flooding. A real situation is that the long wave front trajectory, as a moving wet–dry boundary, is decided by a number of factors, such as external forces, dispersion effect due to wave breaking on steep slopes, etc. External forces usually include gravity, bed friction, wind stress and the Coriolis force in certain circumstances, and they greatly influence the position and movement of water fronts. In addition, a long wave could be dispersed through wave breaking, which also leads to the difficulty in water front prediction. Therefore, the movement of wetting–drying fronts is a highly complex phenomenon and correct simulation of such processes plays a crucial role in practical engineering. Consequently, water flow modelling involving a wet–dry interface has attracted much attention. Hibberd & Peregrine (1979) developed a computational model based on the NLSW equations for wave run-up problems. Liu *et al.* (1995) presented an experimental and numerical study of the interactions of solitary waves climbing up a circular island. Kânoğlu & Synolakis (1998) analytically and experimentally studied long-wave evolution and run-up on piecewise linear bathymetries. Li & Raichlen (2002) investigated solitary wave run-up using the weighted essentially non-oscillatory (WENO) shock capturing scheme. Carrier *et al.* (2003) used a semi-analytic solution technique to evaluate tsunami run-up and draw-down motions on a uniformly sloping beach based on nonlinear shallow-water wave theory.

However, most existing numerical methods for simulating the phenomenon are not based on physical derivation and are unable to correctly include the effect of external forces such as bed friction and wind shear stress on the processes in the simulations, which violates the physics of real flows and undoubtedly introduces further errors in numerical solutions. For example, Kennedy *et al.* (2000) used a so-called 'slot method' and allowed the water level to be below the beach surface, which is apparently not consistent with the real situation. Lynett *et al.* (2002) used a linear extrapolation scheme, which is a pure mathematical manipulation to deal with the wet–dry front. Madsen *et al.* (1997) prescribed a thin water film at a dry bed in the treatment, which is again based on an artificial assumption. Frandsen (2008) incorporated both the linear extrapolation scheme and the thin water film into the 1D lattice Boltzmann shallow-water model to investigate the behaviour of free-surface waves. Finally, Shafiai (2011) adopted similar ideas and conducted intensive simulations using the lattice Boltzmann model for the shallow-water equations.

In addition, there is a Godunov-type method by solving Riemann problems at a wet–dry interface, which is mathematically rigorous. Based on a well-balanced high-order finite volume scheme, Gallardo *et al.* (2007) treated wet–dry fronts through solving specific nonlinear Riemann problems at the corresponding intercells. LeVeque & George (2008) developed a Riemann solver for the shallow-water equations that is able to handle the moving wet–dry interface. George (2008) presented an augmented approximate Riemann solvers for the shallow-water equations, which maintains depth non-negativity and extends naturally to Riemann problems with an initial dry state.

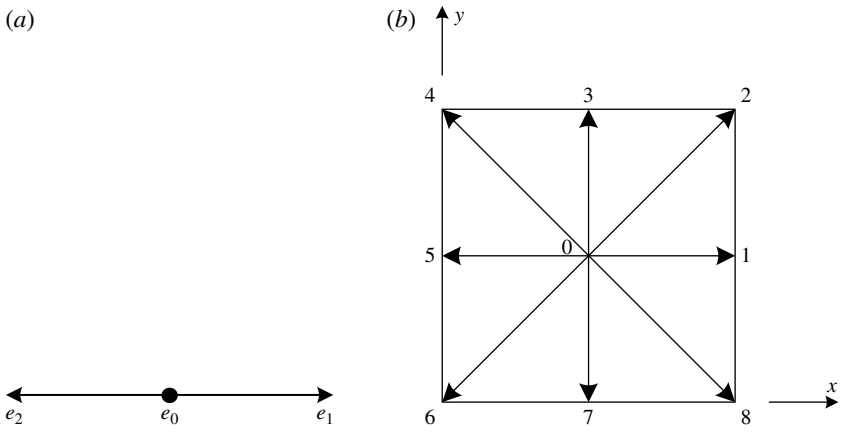

FIGURE 1. Lattice pattern: (*a*) D1Q3; (*b*) D2Q9.

Nevertheless, the algorithms in such schemes are relatively complicated, making it difficult or inefficient to some extent to apply to practical large flow problems.

In this study, we describe a new approach to simulation of the wetting–drying process in the lattice Boltzmann model for shallow-water flows based on the theory of the lattice Boltzmann dynamics. The Chapman–Enskog analysis and the Taylor expansion are applied to set up a relation of the particle distribution functions between a dry bed cell and its neighbouring wet cells in a manner consistent with the LBM. External forces such as bed friction can be included straightforwardly in the approach. The additional advantages of the present scheme are that it does not require a negative water depth like the so-called slot method, or complex Riemann solvers in the Godunov-type method. This new approach may be regarded as a supplement to the LBM for shallow-water flows, which originally cannot automatically deal with the wet–dry interface. Seven numerical tests involving bed friction and different terrains are carried out for its validation.

2. Lattice Boltzmann approach for nonlinear shallow-water equations

In this section, the LBM for NLSW equations is briefly described in one and two dimensions based on D1Q3 and D2Q9 lattices, respectively (see figure 1). As illustrated in (Junk *et al.* 2005), the lattice Boltzmann equation is second-order accurate in space and first-order accurate in time. In the LBM, the streaming and the collision processes can be considered as two separate steps. In the streaming step, the particles move to the neighbouring lattice points in the directions of their individual velocity governed by

$$f_\alpha(\mathbf{x}+\mathbf{e}_\alpha\Delta t, t+\Delta t) = f'_\alpha(\mathbf{x}, t) + W_\alpha \frac{\Delta t}{C_s^2} e_{\alpha i} F_i(\mathbf{x}, t). \tag{2.1}$$

Here f_α is the particle distribution function; f'_α is the value of f_α after collision; $e = \Delta x/\Delta t$; Δx is the lattice size; F_i is the force term in the i direction; Δt is the time step; $\boldsymbol{e}_\alpha$ is the vector of the particle velocity; $e_{\alpha i}$ is the component of $\boldsymbol{e}_\alpha$ (for the D1Q3 lattice (see figure 1(*a*)), $e_0 = 0$, $e_1 = e$ and $e_2 = -e$; for the D2Q9 lattice (see figure 1(*b*)), $\boldsymbol{e}_\alpha$ is defined in table 1); C_s is the local sound speed defined by

$$C_s = \frac{e}{\sqrt{3}}, \tag{2.2}$$

α	0	1	2	3	4	5	6	7	8
$e_{\alpha x}$	0	e	e	0	$-e$	$-e$	$-e$	0	e
$e_{\alpha y}$	0	0	e	e	e	0	$-e$	$-e$	$-e$

TABLE 1. The velocity vector for the D2Q9 lattice.

which is analogous to the kinematic viscosity through (2.9); and W_α is the weighting factor, which for the D1Q3 lattice is 1/4 and for the D2Q9 lattice is given by

$$W_\alpha = \begin{cases} \dfrac{1}{9}, & \alpha = 1, 3, 5, 7, \\ \dfrac{1}{36}, & \alpha = 2, 4, 6, 8. \end{cases} \tag{2.3}$$

In the collision step, considering the simplicity and efficiency and using the Bhatnagar–Gross–Krook (BGK) relaxation term (Bhatnagar *et al.* 1954) as a simple collision operator, the particles arriving at the points interact with one another and f'_α can be written as

$$f'_\alpha(\mathbf{x}, t) = f_\alpha(\mathbf{x}, t) - \frac{1}{\tau}(f_\alpha - f^{eq}_\alpha), \tag{2.4}$$

where f^{eq}_α is the local equilibrium distribution function and τ is the single relaxation time. If f^{eq}_α is computed from either

$$f^{eq}_\alpha = \begin{cases} h - \dfrac{hu^2}{e^2} - \dfrac{gh^2}{2e^2}, & \alpha = 0, \\ \dfrac{gh^2}{4e^2} + \dfrac{hu^2}{2e^2} + \dfrac{hu}{2e}, & \alpha = 1, \\ \dfrac{gh^2}{4e^2} + \dfrac{hu^2}{2e^2} - \dfrac{hu}{2e}, & \alpha = 2, \end{cases} \tag{2.5}$$

for the D1Q3 lattice or

$$f^{eq}_\alpha = \begin{cases} h - \dfrac{5gh^2}{6e^2} - \dfrac{2h}{3e^2}u_i u_i, & \alpha = 0, \\ \dfrac{gh^2}{6e^2} + \dfrac{h}{3e^2}e_{\alpha i}u_i + \dfrac{h}{2e^4}e_{\alpha i}e_{\alpha j}u_i u_j - \dfrac{h}{6e^2}u_i u_i, & \alpha = 1, 3, 5, 7, \\ \dfrac{gh^2}{24e^2} + \dfrac{h}{12e^2}e_{\alpha i}u_i + \dfrac{h}{8e^4}e_{\alpha i}e_{\alpha j}u_i u_j - \dfrac{h}{24e^2}u_i u_i, & \alpha = 2, 4, 6, 8, \end{cases} \tag{2.6}$$

for the D2Q9 lattice, the following NLSW equations can be recovered by using the Chapman–Enskog procedure (Zhou 2004):

$$\frac{\partial h}{\partial t} + \frac{\partial (hu_j)}{\partial x_j} = 0, \tag{2.7}$$

$$\frac{\partial (hu_i)}{\partial t} + \frac{\partial (hu_i u_j)}{\partial x_j} = -\frac{g}{2}\frac{\partial h^2}{\partial x_i} + \nu \frac{\partial^2 (hu_i)}{\partial x_j \partial x_j} + F_i. \tag{2.8}$$

In the above equations, the Cartesian coordinate system and the Einstein summation convention over indices are used; ν is the kinematic viscosity of water defined as

$$\nu = C_s^2 \Delta t \left(\tau - \tfrac{1}{2}\right); \tag{2.9}$$

h is the water depth; x_i and u_i are the distance and the velocity, respectively; and the force F_i is given by

$$F_i = -gh\frac{\partial z_b}{\partial x_i} - \frac{\tau_{bi}}{\rho}, \tag{2.10}$$

where z_b is bed elevation above datum and ρ is fluid density. The bed shear stress τ_{bi} is determined by the depth-averaged velocity

$$\tau_{bi} = \rho C_b u_i \sqrt{u_j u_j}, \tag{2.11}$$

in which C_b is the bed friction coefficient.

From the distribution function, the water depth h and flow velocity u can be calculated from

$$h = \sum_\alpha f_\alpha, \quad u_i = \frac{1}{h}\sum_\alpha e_{\alpha i} f_\alpha. \tag{2.12}$$

3. Treatment of the wet–dry interface

The long-wave run-up and run-down are influenced by a number of factors. The momentum of a wave is mainly depleted by slope gravity and bed friction, whereas wind stress could have a positive or negative effect on wave strength. For a large-scale water body, the Coriolis force should be considered. It can be seen that external forces play an important role in long-wave run-up or run-down. Different from the water body, the wet–dry front of a wave, due to its special position, needs delicate treatment of the external forces in order to correctly model a long-wave run-up and run-down.

3.1. *One-dimensional scheme*

During wetting–drying processes in flows, a cell at or near to the interface between wet and dry cells may become a wet cell when $h > 0$ from a dry cell $h = 0$, and vice versa. In order to treat this properly, we propose a scheme to determine the particle distribution functions at a dry cell based on the dynamics of particles at its neighbouring wet cell, enabling the physical variables at the dry cell to be calculated directly to avoid $h = 0$ in (2.12) when it turns to a wet cell.

As seen in figure 2, nodes d_1 and d_2 (white dots) are within the dry bed, whereas nodes w_1 and w_2 (blue dots) are wet nodes at time t. After one iteration or time step, $f_0^{t+\Delta t}(d_2)$, $f_1^{t+\Delta t}(d_2)$ and $f_1^{t+\Delta t}(w_1)$ (shown in red) are still unknown at the wet–dry interface. In order to obtain $f_1^{t+\Delta t}(w_1)$ at $t + \Delta t$, one has to be calculate $f_1^t(d_2)$. Although d_2 initially is dry, i.e. $f_1^{t,eq}(d_2) = 0$, the $f_1^t(d_2)$ can be derived through the non-equilibrium part of the particle distribution function $f_1^{t,neq}(d_2)$.

Setting $\Delta t = \varepsilon$ and applying the Taylor expansion to the first term on the left-hand side of (2.1) in time and space at point (x, t) results in

$$\varepsilon\left(\frac{\partial}{\partial t} + e_\alpha\frac{\partial}{\partial x}\right)f_\alpha + \frac{\varepsilon^2}{2}\left(\frac{\partial}{\partial t} + e_\alpha\frac{\partial}{\partial x}\right)^2 f_\alpha + o(\varepsilon^3) = -\frac{1}{\tau}(f_\alpha - f_\alpha^{(0)}) + \frac{\Delta t}{2e^2}e_\alpha F, \tag{3.1}$$

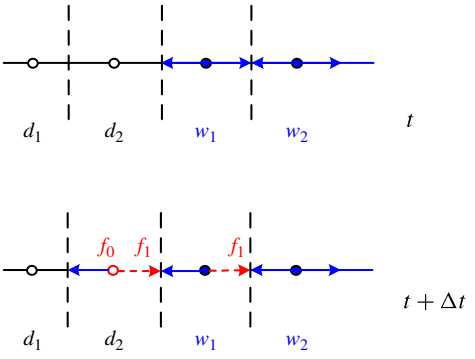

FIGURE 2. (Colour online) Sketch of the one-dimensional wet–dry interface (d and w denote dry and wet cells, respectively).

where $f_\alpha^{(0)} = f_\alpha^{eq}$. Also, f_α can be expanded around $f_\alpha^{(0)}$ using the Chapman–Enskog expansion

$$f_\alpha = f_\alpha^{(0)} + \varepsilon f_\alpha^{(1)} + o(\varepsilon^2). \tag{3.2}$$

If higher orders of ε are neglected, substitution of (3.2) into (3.1) leads to

$$\begin{aligned} &\varepsilon\left(\frac{\partial}{\partial t} + e_\alpha\frac{\partial}{\partial x}\right)(f_\alpha^{(0)} + \varepsilon f_\alpha^{(1)}) + \frac{\varepsilon^2}{2}\left(\frac{\partial}{\partial t} + e_\alpha\frac{\partial}{\partial x}\right)^2(f_\alpha^{(0)} + \varepsilon f_\alpha^{(1)}) \\ &= -\frac{1}{\tau}f_\alpha^{(1)} + \frac{\Delta t}{2e^2}e_\alpha F. \end{aligned} \tag{3.3}$$

The above equation to order ε is

$$\left(\frac{\partial}{\partial t} + e_\alpha\frac{\partial}{\partial x}\right)f_\alpha^{(0)} = -\frac{1}{\tau}f_\alpha^{(1)} + \frac{e_\alpha F}{2e^2}. \tag{3.4}$$

For the dry bed cell, because

$$f_\alpha^{(0)} = 0, \tag{3.5}$$

and using the backward scheme

$$\frac{\partial f_\alpha^{(0)}}{\partial t} = \frac{f_\alpha^{(0)}(t) - f_\alpha^{(0)}(t-1)}{\Delta t} = 0, \tag{3.6}$$

from (3.4), one can derive that

$$f_\alpha^{(1)} = \tau\left(\frac{1}{2e^2}e_\alpha F - e_\alpha\frac{\partial f_\alpha^{(0)}}{\partial x}\right). \tag{3.7}$$

With reference to (2.10), (3.5) and (3.6), after (3.7) is put into (3.2), one can obtain the particle distribution function as

$$f_\alpha = f_\alpha^{(0)} + \varepsilon f_\alpha^{(1)} = \varepsilon\tau\left(\frac{1}{2e^2}e_\alpha\left(-gh\frac{\partial z_b}{\partial x} - \frac{\tau_b}{\rho}\right) - e_\alpha\frac{\partial f_\alpha^{(0)}}{\partial x}\right), \tag{3.8}$$

in which

$$\frac{\partial z_b}{\partial x} = \frac{z_b(x + e_\alpha \Delta t) - z_b(x)}{e_\alpha \Delta t} \tag{3.9}$$

and

$$\frac{\partial f_\alpha^{(0)}}{\partial x} = \frac{f_\alpha^{(0)}(x + e_\alpha \Delta t) - f_\alpha^{(0)}(x)}{e_\alpha \Delta t}. \tag{3.10}$$

If ε is replaced with Δt, substitution of (3.9) and (3.10) into (3.8) results in

$$f_\alpha = \frac{-gh\tau}{2e^2}(z_b(x + e_\alpha \Delta t) - z_b(x)) - \frac{\Delta t \tau}{2e^2} e_\alpha C_b u|u| - \tau(f_\alpha^{(0)}(x + e_\alpha \Delta t) - f_\alpha^{(0)}(x)). \tag{3.11}$$

Equation (3.11) can be used to determine $f_1^t(d_2)$, provided that $f_2^t(d_2)$ is positive, i.e. the fluid at w_1 has enough momentum to reach the neighbouring dry node. Otherwise, the standard bounce-back scheme is used to compute $f_1^t(d_2)$, which leads to first-order accuracy of the solution in an arbitrary domain. One can calculate $f_0^t(d_2)$ by the average f_0^t of its neighbouring nodes as

$$f_0^t(d_2) = \frac{f_0^t(d_1) + f_0^t(w_1)}{2}. \tag{3.12}$$

Using (2.12) will decide if the dry node d_2 remains dry if $h \leqslant 0$ or becomes wet if $h > 0$, for which the velocity can further be calculated from the equation. The opposite situation whether wet cell w_1 becomes dry or not can be similarly determined. It may be noted that this approach is a consistent extension of the LBM to simulating wetting–drying processes without a non-physical assumption, which has a unique advantage of natural and straightforward incorporation of an additional external force for the phenomenon in complex flows.

3.2. *Two-dimensional case*

The extension of the 1D scheme to the 2D framework on Cartesian meshes is straightforward. As the effect of the bed slope is usually anisotropic in shallow-water modelling, the bed level is incorporated into the lattice Boltzmann equation to improve the accuracy and eliminate the calculation of the derivative related to the bed slope (Zhou 2011). As seen from (2.10), F_i contains a first derivative related to the bed level, which is inconsistent with simple arithmetic calculations required in the lattice Boltzmann hydrodynamics. In order to overcome the drawback, the lattice Boltzmann (2.1) is modified as

$$\begin{aligned} &f_\alpha(\mathbf{x} + \mathbf{e}_\alpha \Delta t, t + \Delta t) \\ &\quad = f_\alpha(\mathbf{x}, t) - \frac{1}{\tau}(f_\alpha(x, t) - f_\alpha^{eq}(x, t)) - W_\alpha \frac{g\bar{h}}{C_s^2}(z_b(\mathbf{x} + \mathbf{e}_\alpha \Delta t) - z_b(\mathbf{x})) \\ &\qquad + W_\alpha \frac{\Delta t}{C_s^2} e_{\alpha i} F_i, \end{aligned} \tag{3.13}$$

where $\bar{h} = (h(\mathbf{x} + \mathbf{e}_\alpha \Delta t, t + \Delta t) + h(\mathbf{x}, t))/2$.

Assuming that Δt is small and $\varepsilon = \Delta t$, (3.13) can be expressed as

$$\begin{aligned} & f_\alpha(\mathbf{x} + \mathbf{e}_\alpha \varepsilon, t + \varepsilon) \\ & \quad = f_\alpha(\mathbf{x}, t) - \frac{1}{\tau}(f_\alpha(x, t) - f_\alpha^{eq}(x, t)) - W_\alpha \frac{g\bar{h}}{C_s^2}(z_b(\mathbf{x} + \mathbf{e}_\alpha \varepsilon) - z_b(\mathbf{x})) \\ & \qquad + W_\alpha \frac{\varepsilon}{C_s^2} e_{\alpha i} F_i. \end{aligned} \tag{3.14}$$

Taking a Taylor expansion of the left-hand side of the above equation in time and space around point (x, t) leads to

$$\begin{aligned} & \varepsilon \left(\frac{\partial}{\partial t} + e_\alpha \frac{\partial}{\partial x_j} \right) f_\alpha + \frac{\varepsilon^2}{2} \left(\frac{\partial}{\partial t} + e_\alpha \frac{\partial}{\partial x_j} \right)^2 f_\alpha + o(\varepsilon^3) \\ & \quad = -\frac{1}{\tau}(f_\alpha(x, t) - f_\alpha^{eq}(x, t)) - W_\alpha \frac{g\bar{h}}{C_s^2}(z_b(x + e_\alpha \varepsilon) - z_b(x)) + W_\alpha \frac{\varepsilon}{C_s^2} e_{\alpha i} F_i. \end{aligned} \tag{3.15}$$

Using the Chapman–Enskog procedure again, f_α can be expanded around $f_\alpha^{(0)}$,

$$f_\alpha = f_\alpha^{(0)} + \varepsilon f_\alpha^{(1)} + \varepsilon^2 f_\alpha^{(2)} + o(\varepsilon^3). \tag{3.16}$$

If the Taylor expansion is also applied to the second term and the force term F_i on the right-hand side of (3.14), one can obtain

$$W_\alpha \frac{g}{C_s^2} \left(h + \frac{\varepsilon}{2} \left(\frac{\partial h}{\partial t} + e_{\alpha j} \frac{\partial h}{\partial x_j} \right) \right) \left(\varepsilon e_{\alpha j} \frac{\partial z_b}{\partial x_j} + \frac{\varepsilon^2}{2} e_{\alpha i} e_{\alpha j} \frac{\partial^2 z_b}{\partial x_i x_j} \right) + o(\varepsilon^3) \tag{3.17}$$

and

$$F_i = F_i \left(\mathbf{x} + \frac{1}{2}\mathbf{e}_\alpha \varepsilon, \;\; t + \frac{1}{2}\varepsilon \right) = F_i + \frac{\varepsilon}{2} \left(\frac{\partial F_i}{\partial t} + e_\alpha \frac{\partial F_i}{\partial x_i} \right) + o(\varepsilon^2), \tag{3.18}$$

in which the centred scheme is used for force term F_i (Zhou 2004). After inserting (3.16)–(3.18) into (3.15), the equation to order ε^0 is

$$f_\alpha^{(0)} = f_\alpha^{eq}, \tag{3.19}$$

to order ε^1 is

$$\left(\frac{\partial}{\partial t} + e_{\alpha j} \frac{\partial}{\partial x_j} \right) f_\alpha^{(0)} = -\frac{1}{\tau} f_\alpha^{(1)} - W_\alpha \frac{g h e_{\alpha j}}{C_s^2} \frac{\partial z_b}{\partial x_j} + W_\alpha \frac{e_{\alpha j} F_j}{C_s^2} \tag{3.20}$$

and to order ε^2 is

$$\begin{aligned} & \left(\frac{\partial}{\partial t} + e_{\alpha j} \frac{\partial}{\partial x_j} \right) f_\alpha^{(1)} + \frac{1}{2} \left(\frac{\partial}{\partial t} + e_{\alpha j} \frac{\partial}{\partial x_j} \right)^2 f_\alpha^{(0)} \\ & \quad = -\frac{1}{\tau} f_\alpha^{(2)} - W_\alpha \frac{g e_{\alpha j}}{2C_s^2} \left(\frac{\partial h}{\partial t} + e_{\alpha i} \frac{\partial h}{\partial x_i} \right) \frac{\partial z_b}{\partial x_j} - W_\alpha \frac{g h e_{\alpha i} e_{\alpha j}}{2C_s^2} \frac{\partial^2 z_b}{x_i x_j} \\ & \qquad + W_\alpha \frac{e_{\alpha i}}{2C_s^2} \left(\frac{\partial F_i}{\partial t} + e_{\alpha j} \frac{\partial F_i}{\partial x_i} \right). \end{aligned} \tag{3.21}$$

Substitution of (3.20) into (3.21) and rearrangement produces

$$\left(1-\frac{1}{2\tau}\right)\left(\frac{\partial}{\partial t}+e_{\alpha j}\frac{\partial}{\partial x_j}\right)f_\alpha^{(1)}=-\frac{1}{\tau}f_\alpha^{(2)}. \tag{3.22}$$

Taking $\sum_\alpha((3.20)+\varepsilon\times(3.22))$ provides

$$\frac{\partial}{\partial t}\sum_\alpha f_\alpha^{(0)}+\frac{\partial}{\partial x_j}\sum_\alpha e_{\alpha j}f_\alpha^{(0)}=0. \tag{3.23}$$

Evaluation of the terms in the above equation using (2.6) results in the second-order accurate continuity (2.7).

Then, taking $\sum_\alpha e_{\alpha i}((3.20)+\varepsilon\times(3.22))$, one can obtain

$$\begin{aligned}&\frac{\partial}{\partial t}\sum_\alpha e_{\alpha i}f_\alpha^{(0)}+\frac{\partial}{\partial x_j}\sum_\alpha e_{\alpha i}e_{\alpha j}f_\alpha^{(0)}+\varepsilon\left(1-\frac{1}{2\tau}\right)\frac{\partial}{\partial x_j}\sum_\alpha e_{\alpha i}e_{\alpha j}f_\alpha^{(1)}\\&\quad=F_i-gh\frac{\partial z_b}{\partial x_i}.\end{aligned} \tag{3.24}$$

After the terms are evaluated with (2.6) and some algebra, the above equation becomes another form of the momentum equations (2.8),

$$\frac{\partial(hu_i)}{\partial t}+\frac{\partial(hu_iu_j)}{\partial x_j}=-\frac{g}{2}\frac{\partial h^2}{\partial x_i}-gh\frac{\partial z_b}{\partial x_i}+\nu\frac{\partial^2(hu_i)}{\partial x_j\partial x_j}+F_i, \tag{3.25}$$

which is second-order accurate with F_i. The following semi-implicit form is used for determining $\bar{h}$ in order to eliminate the implicitness,

$$\bar{h}=\frac{1}{2}(h(\mathbf{x}+\mathbf{e}_\alpha\Delta t,\,t)+h(\mathbf{x},\,t)), \tag{3.26}$$

which is simple and demonstrated to produce accurate solutions and hence it is preferred in practice (Zhou 2004).

Since, in a lattice Boltzmann model, rotational symmetry and moment isotropy are satisfied up to fourth order (Chen *et al.* 2008), the proposed technique for the one-dimensional case can be applied to the two-dimensional case in both diagonal and off-diagonal directions. Two cases for a dry node at wet–dry boundaries with $n<4$ and $n\geqslant 4$ are illustrated in figure 3, where n denotes the number of wet-neighbouring nodes. The unknown distribution functions at dry nodes moving towards wet nodes can be calculated using (3.27), which is similar to (3.11), i.e. for $\alpha=1,2,8$ at $t+\Delta t$ in figure 3(*a*), we have

$$\begin{aligned}f_\alpha\;=\;&\frac{-W_\alpha gh\tau}{C_s^2}(z_b(\mathbf{x}+\mathbf{e}_\alpha\Delta t)-z_b(\mathbf{x}))-\frac{W_\alpha\Delta t\tau}{C_s^2}e_{\alpha i}C_bu_i\sqrt{u_ju_j}\\&-\tau(f_\alpha^{(0)}(\mathbf{x}+\mathbf{e}_\alpha\Delta t)-f_\alpha^{(0)}(\mathbf{x})).\end{aligned} \tag{3.27}$$

However, there may still be additional unknown distribution functions without facing wet nodes in their moving directions, like f_3 and f_7 at the interface shown in figure 3(*a*). In this case, they can be obtained by using the average value of its

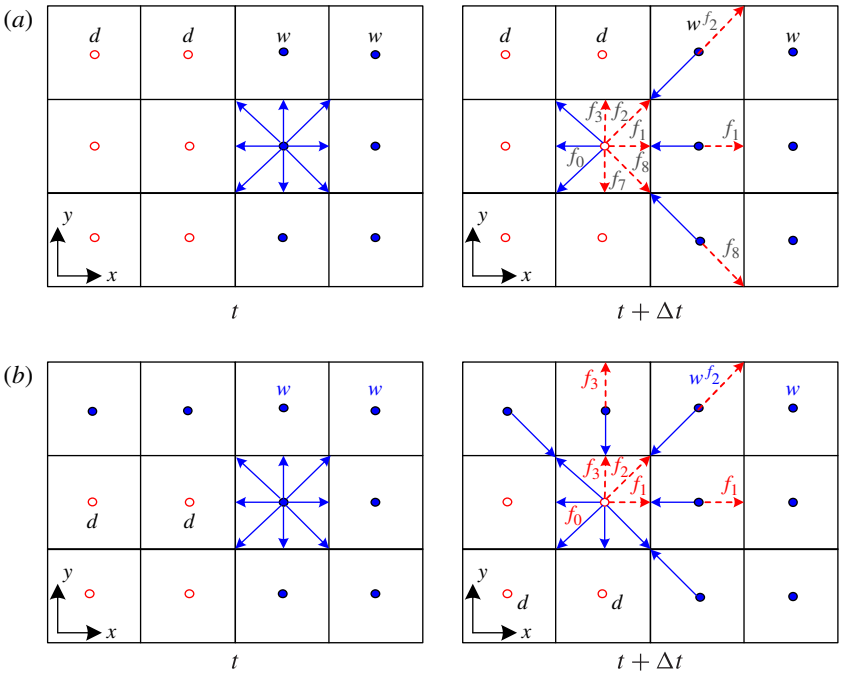

FIGURE 3. (Colour online) Sketch of the two-dimensional wet–dry interface (d and w denote dry and wet cells, respectively; and n is the number of the neighbouring wet nodes of a dry node): (*a*) $n < 4$; (*b*) $n \geqslant 4$.

neighbouring nodes as in (3.28), which is necessary for $n < 4$. When $n \geqslant 4$ as depicted in figure 3(*b*), only f_0 is unknown and needs to be calculated by

$$f_\alpha = \frac{1}{8}\sum_{\beta=1}^{8} f_\alpha(\mathbf{x} + \mathbf{e}_\beta \Delta t). \tag{3.28}$$

The solution procedure for the scheme involves only explicit calculations, which makes programming easy and efficient. In general, it includes the following steps:

1. Set initial values of u and h within the wet domain.
2. Calculate f_α^{eq} from (2.5) or (2.6) for each wet cell.
3. If $f_{\bar{\alpha}} > 0$ at the dry cell next to the wet–dry interface ($\bar{\alpha}$ stands for the direction from wet cell to dry cell, i.e. the opposite direction to α), calculate f_α at the dry cell from (3.11) and (3.12) in one dimension or from (3.27) and (3.28) in two dimensions. Otherwise, the standard bounce-back scheme is used.
4. Calculate f_α at both collision and streaming steps through the lattice Boltzmann (2.1) with the relaxation time τ.
5. Use step 3 again to supplement the unknown f_α at $t + \Delta t$ at the dry cell.
6. Update u and h using (2.12) within the wet domain.
7. Return to step 2 and repeat the above steps until the solution of the desired target time is obtained.

4. Verification

4.1. *Sloshing over a 1D parabolic container*

Analytical solutions of the NLSW equations for perturbed flow in a container with parabolic bed topography and bed friction were derived by Sampson *et al.* (2006). It is a very useful benchmark test for validating the wetting and drying process in a numerical model. Since bed friction and bed slope are involved, the analytical solutions can also be used to verify the scheme involving force terms. As stated in Sampson *et al.* (2006), the bed profile of the domain is defined by

$$z_b(x) = h_0 \left(\frac{x}{a}\right), \tag{4.1}$$

in which z_b is uniform in the y direction, and h_0 and a are constants. A bed friction parameter τ_b is related to the bed friction coefficient as

$$C_b = \frac{h\tau_b}{|u|}, \tag{4.2}$$

and a hump amplitude parameter $p = \sqrt{8gh_0}/a$ is used in the analytical solutions of the water surface above a horizontal datum,

$$\begin{aligned}\eta(x,t) \;=\; & h_0 + \frac{a^2B^2\mathrm{e}^{-\tau_b t}}{8g^2h_0}\left(-s\tau_b \sin 2st + \left(\frac{\tau_b^2}{4} - s^2\right)\cos 2st\right) - \frac{B^2\mathrm{e}^{\tau_b t}}{4g} \\ & - \frac{\mathrm{e}^{\tau_b t/2}}{g}\left(Bs\cos st + \frac{\tau_b B}{2}\sin st\right)x,\end{aligned} \tag{4.3}$$

where B is a constant and $s = \sqrt{p^2 - \tau_b^2}/2$. When $t \to \infty$, (4.3) defines the still-water elevation above the datum, i.e. $\eta(t) \to h_0$. The moving shorelines actually are two parallel straight lines on the horizontal plane and could be calculated by

$$x = -\frac{a^2\mathrm{e}^{-\tau_b t/2}}{2gh_0}\left(Bs\cos st + \frac{\tau_b B}{2}\sin st\right) \pm a. \tag{4.4}$$

The oscillatory flow is damped due to bed friction, resulting in $x \to a$ as $t \to \infty$.

The computations are carried out using a uniform lattice with 200 nodes over a 10 000 m domain. The coefficients involved in the simulation are $h_0 = 10$ m, $a = 3$ km, $\tau_b = 0.001$ s^{-1} and $B = 5$ m s^{-1}. The simulation lasts 6000 s and the time step Δt is 0.5 s. Initially, the water surface is set according to (4.3) and the velocity is zero. As presented in figure 4, the moving wet–dry interfaces caused by the sloshing motions are well reproduced, thus validating the new approach to treat the wet–dry interface as well as the accuracy of calculating the force terms.

4.2. *A 1D tidal wave over a variable sloping bed*

This example was proposed initially by Leclerc *et al.* (1990) with the purpose of reproducing the shoreline movement under a tide over a variable sloping bed. The channel is 500 m long and the slope ($S = \partial z_b/\partial x$) in the longitudinal direction is given in table 2.

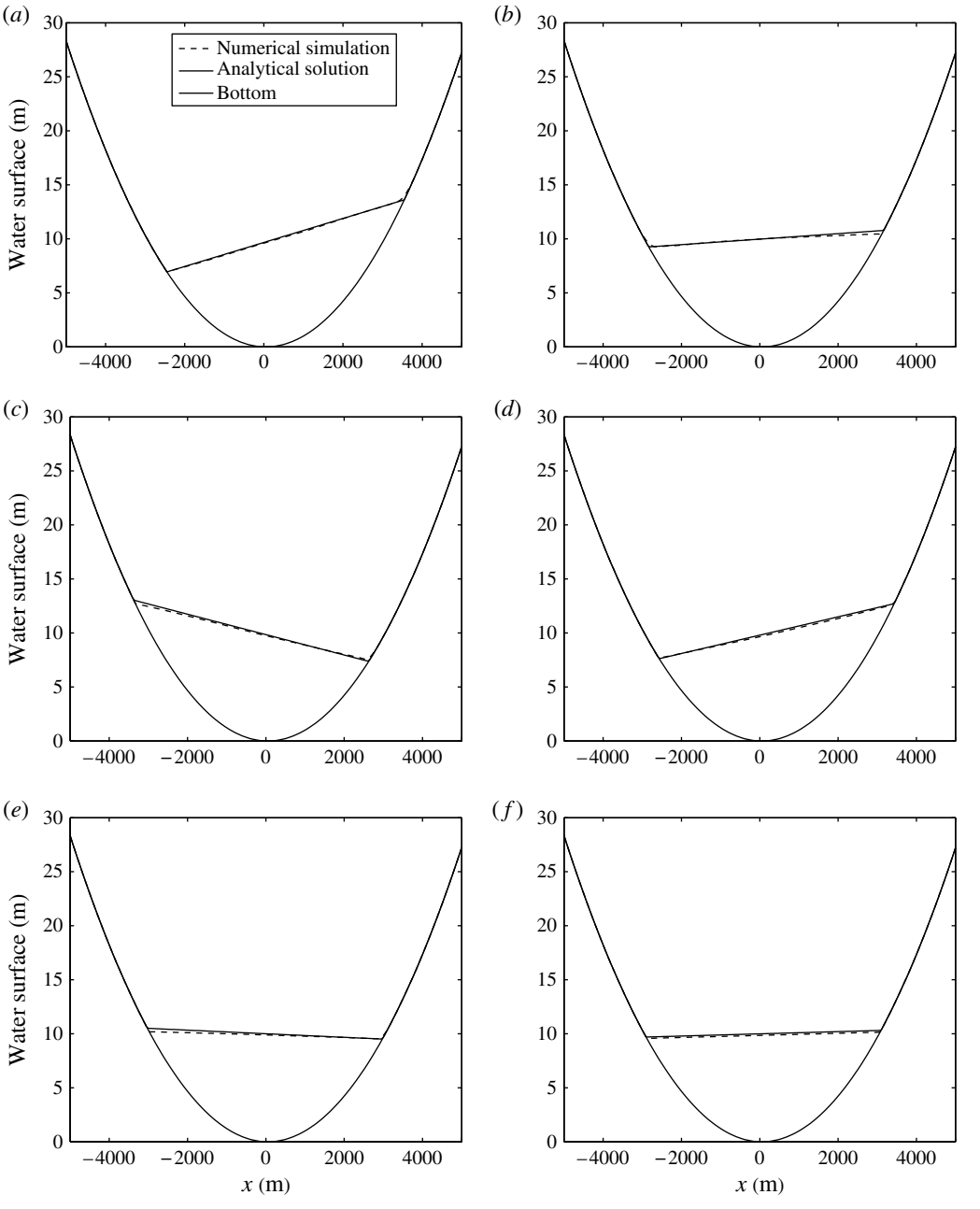

FIGURE 4. Comparisons of the water surface for sloshing motions: (*a*) $t = 500$ s; (*b*) $t = 1000$ s; (*c*) $t = 1500$ s; (*d*) $t = 2000$ s; (*e*) $t = 3000$ s; (*f*) $t = 6000$ s.

A steady state with the water level of 1.75 m is considered as the initial condition. The solid boundary is set at $x = 0$ m and the inlet boundary at $x = 500$ m is associated with the variation of the water depth following the tide (see figure 5) as

$$h(500, t) = h_0 + \lambda \cos\left(2\pi \frac{t}{T}\right), \tag{4.5}$$

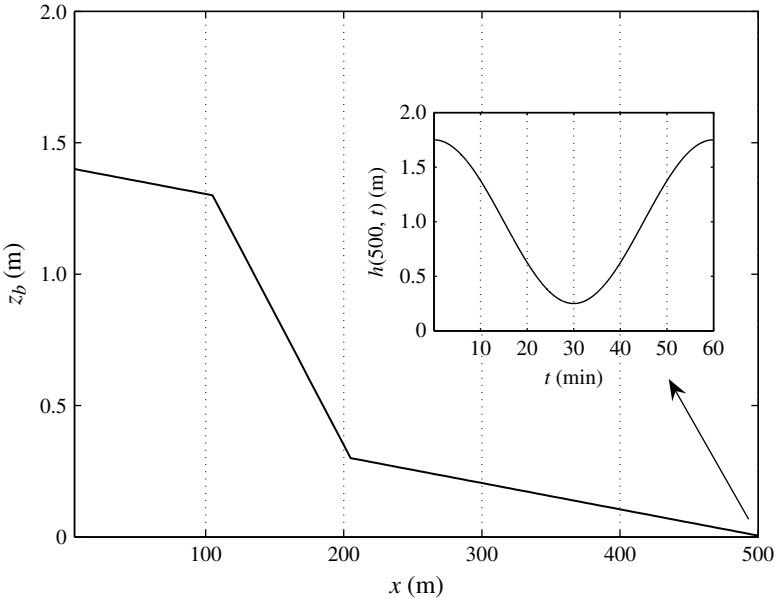

FIGURE 5. Bed elevation and inlet boundary condition.

x (m)	0–100	100–200	200–500
S	−0.001	−0.01	−0.001

TABLE 2. Bed slopes.

where $h_0 = 1$ m is the reference water surface, $\lambda = 0.75$ m is the amplitude of the tidal wave and $T = 3600$ s is the tidal period. In addition, $n = 0.03$ is taken as the Manning roughness coefficient. According to the study by Brufau *et al.* (2002), the computational domain is covered with 100 lattices. Several values of the single relaxation time τ are tested, as shown in figure 6. Compared with the well-documented numerical tests by Leclerc *et al.* (1990) referred to as the reference data in figure 6 and Heniche *et al.* (2000), the results based on $\tau = 0.7$ agree well and hence are taken for further study. The water surface and the velocity are depicted in figure 7. The results are very close to those obtained by Leclerc *et al.* (1990) and Heniche *et al.* (2000), who used a completely different numerical algorithm based on finite element methods, and the accuracy is improved compared with those computed by Brufau *et al.* (2002), who used a finite volume type of technique. These results have well illustrated the capability of the proposed model to reproduce both temporal and spatial movement of the wetting–drying interface.

4.3. *A 1D solitary wave run up over a plane sloping beach*

Disastrous geophysical activities such as seabed earthquakes and extensive landslides may cause massive displacement of the water surface, resulting in huge long waves, which are known to cause extensive flooding and loss of life (Titov & Synolakis 1995). Such disastrous waves can be approximated as a solitary wave (Synolakis 1987;

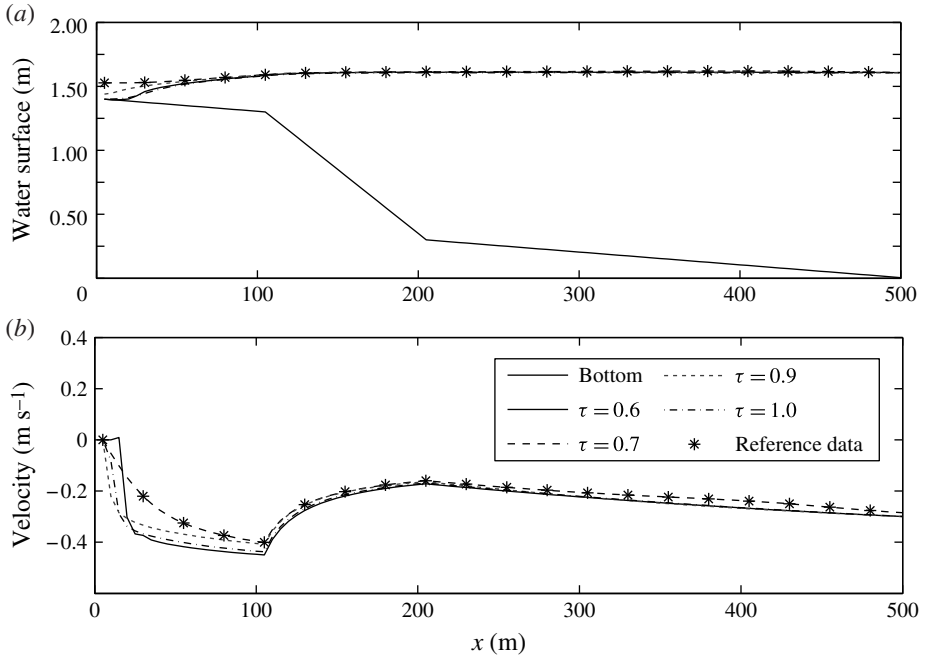

FIGURE 6. Comparisons of (*a*) the water level and (*b*) the velocity for different values of τ at time $t = 54$ min.

Mahdavi & Talebbeydokhti 2009). A detailed experimental study of solitary wave run up on a plane beach has been undertaken by Synolakis (1986), in which the run-up of non-breaking and breaking solitary waves are intensively investigated. A number of researchers used his data for validating numerical models (Zelt 1991; Rogers *et al.* 2001; Mahdavi & Talebbeydokhti 2009). In the present study, an incident wave of $H/h_0 = 0.0185$ is considered with a beach slope of 1/19.85, where H is the solitary wave height, h_0 is the still-water level, θ is the beach slope, R is the run-up height measured above the still-water level and L is the wavelength (see figure 8).

The initial wave crest of the solitary wave is located at a distance x_0 from the toe of the beach and the wave height can be defined as

$$\eta(x, 0) = \frac{H}{h_0} \operatorname{sech}^2 \left(\sqrt{\frac{3H}{4h_0}} (x - x_0) \right), \tag{4.6}$$

where x_0 may be computed by

$$x_0 = \sqrt{\frac{4D}{3H}} \operatorname{arccosh} \left(\sqrt{\frac{1}{0.05}} \right). \tag{4.7}$$

In addition, the velocity is given by

$$u(x, 0) = \eta(x, 0) \sqrt{\frac{g}{h_0}} \tag{4.8}$$

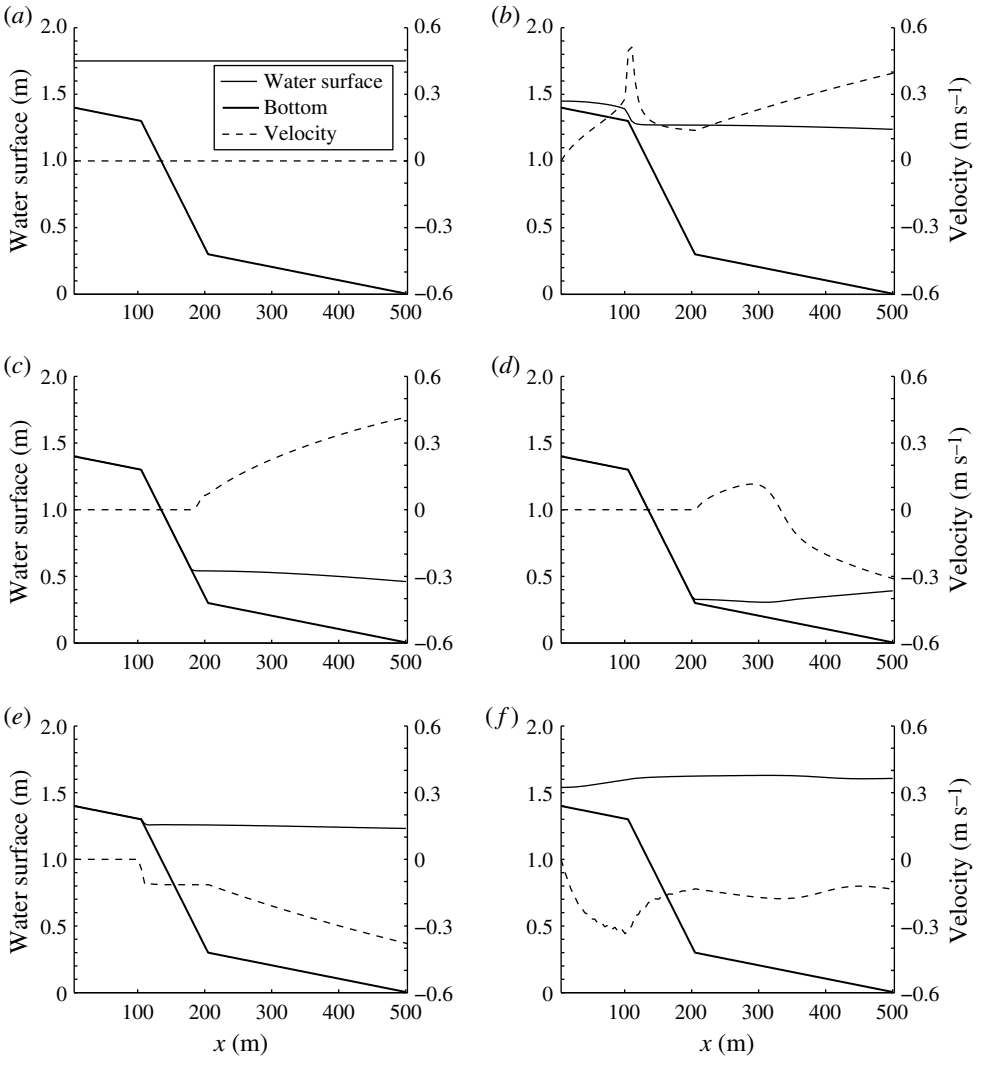

FIGURE 7. Snapshots of the wet–dry fronts for a tide over a variable bed: (*a*) $t = 0$ min; (*b*) $t = 12$ min; (*c*) $t = 24$ min; (*d*) $t = 36$ min; (*e*) $t = 48$ min; (*f*) $t = 54$ min.

and the non-dimensional time is defined as

$$t^* = t\sqrt{\frac{g}{h_0}}. \tag{4.9}$$

For comparison purposes, the same parameters as those used by Shafiai (2011) are also taken in the present numerical simulation, i.e. $\tau = 1$, $\Delta t = 0.01$ s and $\Delta x = 0.05$ m. A constant Manning roughness coefficient $n = 0.01$ is commonly used in practice, although it may introduce some errors into an unsteady and non-uniform problem. This can be used to estimate the friction coefficient $C_b = g/C_z$ through the Chézy coefficient $C_z = h^{1/6}/n$. Snapshots of water surface elevation are presented in figure 9. Compared with the experimental data, the model with the proposed

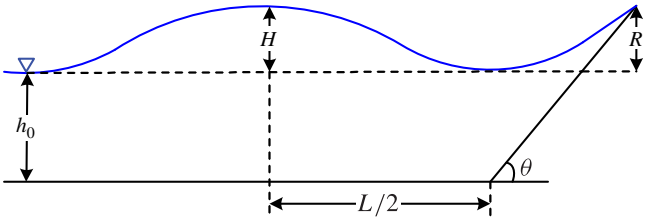

FIGURE 8. (Colour online) Sketch of solitary wave run up on a plane sloping beach.

Time	Thin film	Linear extrapolation	Proposed technique
$t^* = 35$	0.0173	0.0173	0.0172
$t^* = 50$	0.0675	0.0368	0.0184
$t^* = 70$	0.0767	0.0265	0.0243

TABLE 3. The average error of water depth for three techniques investigated.

technique for treating the wet–dry front generates accurate results in the whole process of the solitary wave run-up and run-down. In figure 10, the results of the present scheme, the thin-film technique and the linear extrapolation technique are compared. As shown, the proposed technique not only improves the wet–dry front prediction by providing water surfaces in good agreement with the experimental data, but also predicts excellent trends and a more realistic wet–dry front, whereas the other methods undershoot the run-up heights and produce wrong run-up trends. If the differences between the numerical results and the experimental data are quantified by the average error, the results obtained by the proposed technique are an improvement, as shown in table 3 for $t^* = 35$, 50 and 70. In order to quantify the effect of the bed friction, the surface elevations predicted using different Manning coefficients at $t^* = 50$ are presented in figure 11. It shows that the wave run-up height becomes lower with the increase of the bed friction, which correctly reflects the effect of bed friction on wave run-up, further demonstrating the advantage of the proposed scheme over existing methods.

4.4. *Tsunami run up on a plane beach*

This test represents a tsunami wave running up and drawing down on a plane beach, which was initially semi-analytically studied by Carrier *et al.* (2003). It is also used to verify numerical schemes by Frandsen (2008) and Delis *et al.* (2008). The initial shoreline position is located at $x = 0$ m. A tsunami wave is induced by a non-zero initial water surface with flow velocity equal to zero. The slope of the beach is a constant 0.1. The form of the leading depression N-shaped wave (see figure 12), caused by a submarine landslide, can be described by

$$\eta = a_1 \mathrm{e}^{-k_1(x-x_1)^2} - a_2 \mathrm{e}^{-k_2(x-x_2)^2}, \tag{4.10}$$

where $a_1 = a_2/3 = 0.006$, $k_1 = 0.4444$, $k_2 = 4$, $x_1 = 4.1209$ and $x_2 = 1.6384$, as indicated by Carrier *et al.* (2003).

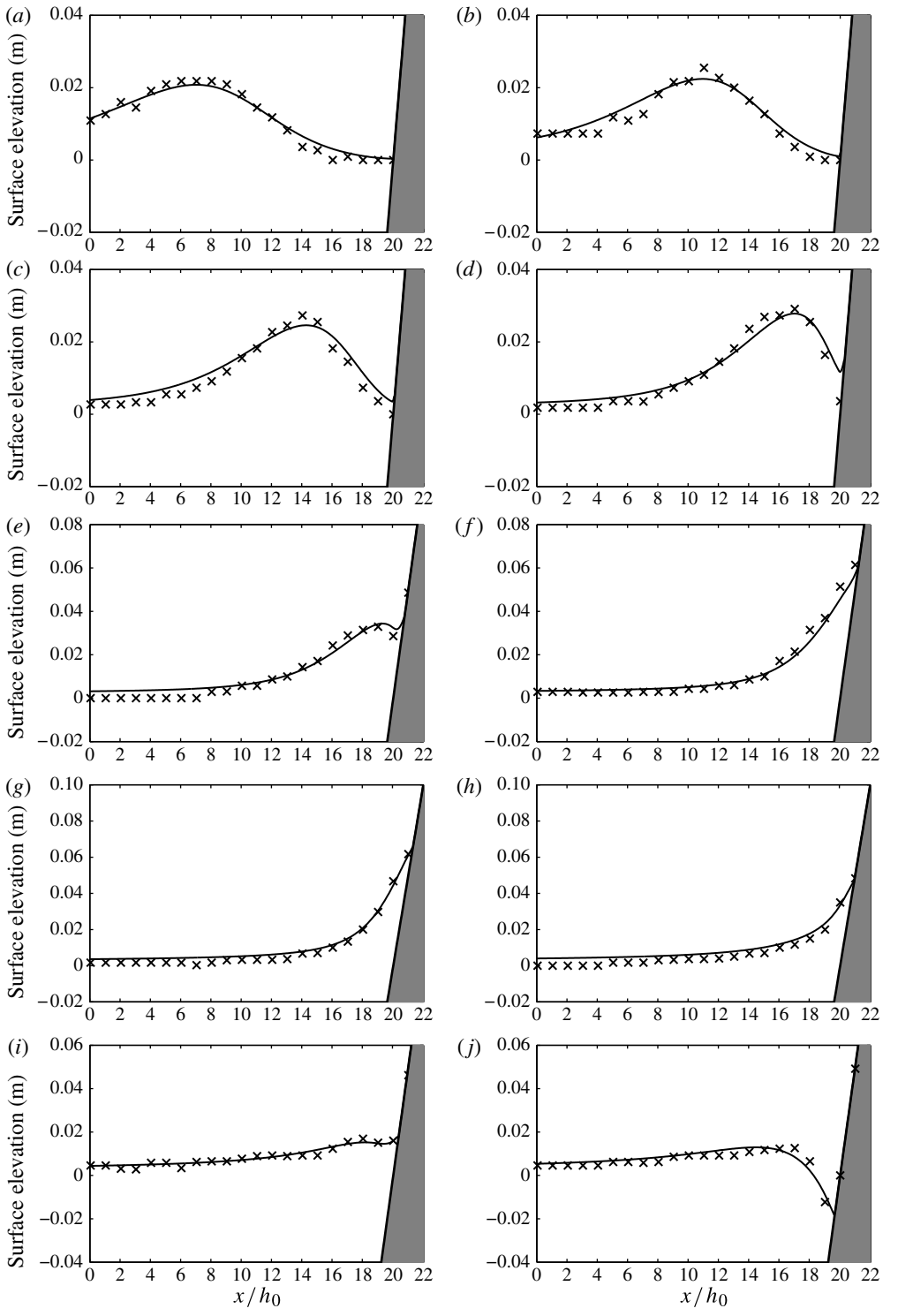

FIGURE 9. Comparisons of the water surface for the run-up process of a solitary wave: (*a*) $t^* = 25$; (*b*) $t^* = 30$; (*c*) $t^* = 35$; (*d*) $t^* = 40$; (*e*) $t^* = 45$; (*f*) $t^* = 50$; (*g*) $t^* = 55$; (*h*) $t^* = 60$; (*i*) $t^* = 65$; (*j*) $t^* = 70$.

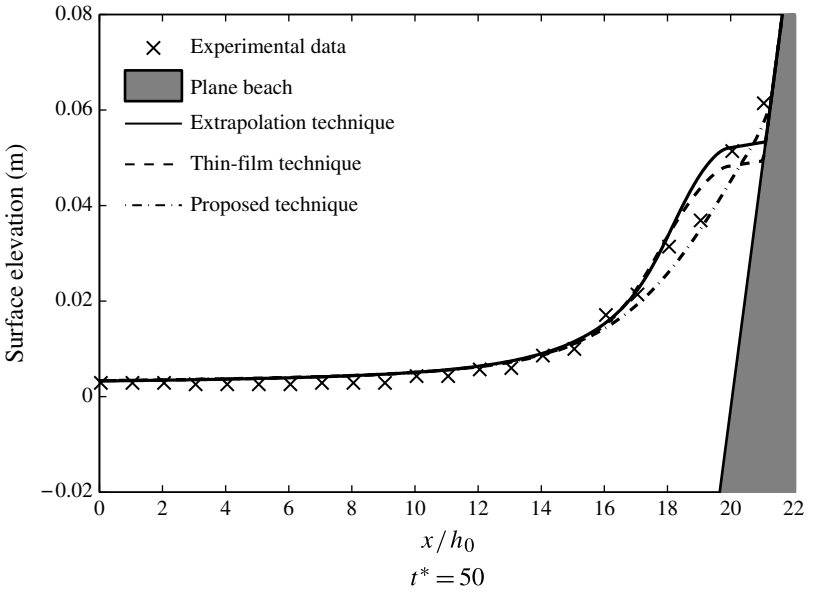

FIGURE 10. Comparisons of the water surfaces generated by using different numerical techniques.

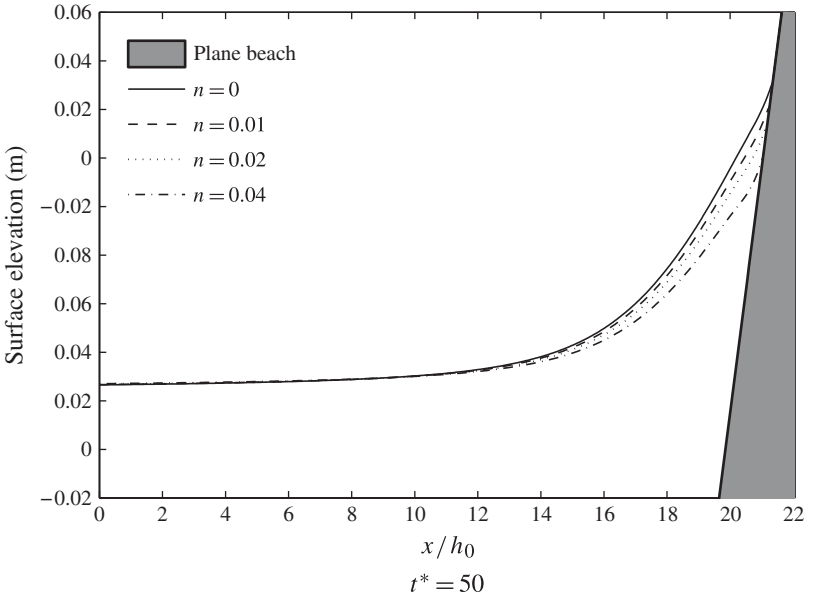

FIGURE 11. Effect of bed friction on wave run-up by using different Manning coefficients.

The computational domain $x \in [-500\ \text{m}, 50\,000\ \text{m}]$ is divided into 100 000 uniform lattices. The time step Δt is set to 0.002 s. The computational time is taken up to 350 s. The water surface and velocity obtained from the numerical scheme are compared with the exact result by Carrier *et al.* (2003). Overall, the numerical result based on the proposed scheme is close to the analytical solution. Figure 13 shows

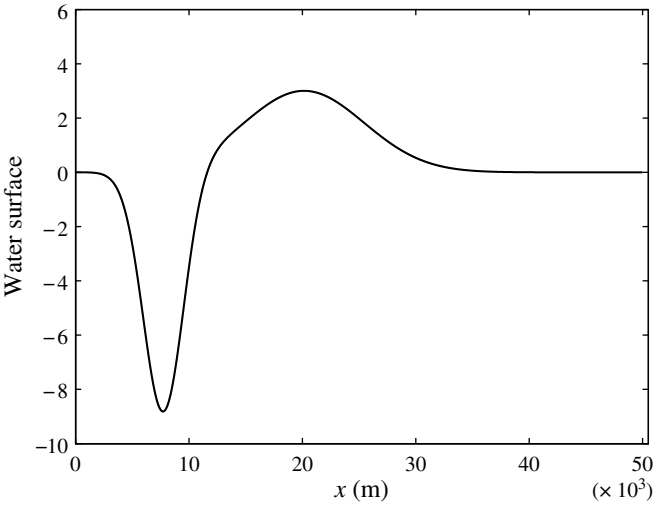

FIGURE 12. Initial water surface condition for tsunami run-up.

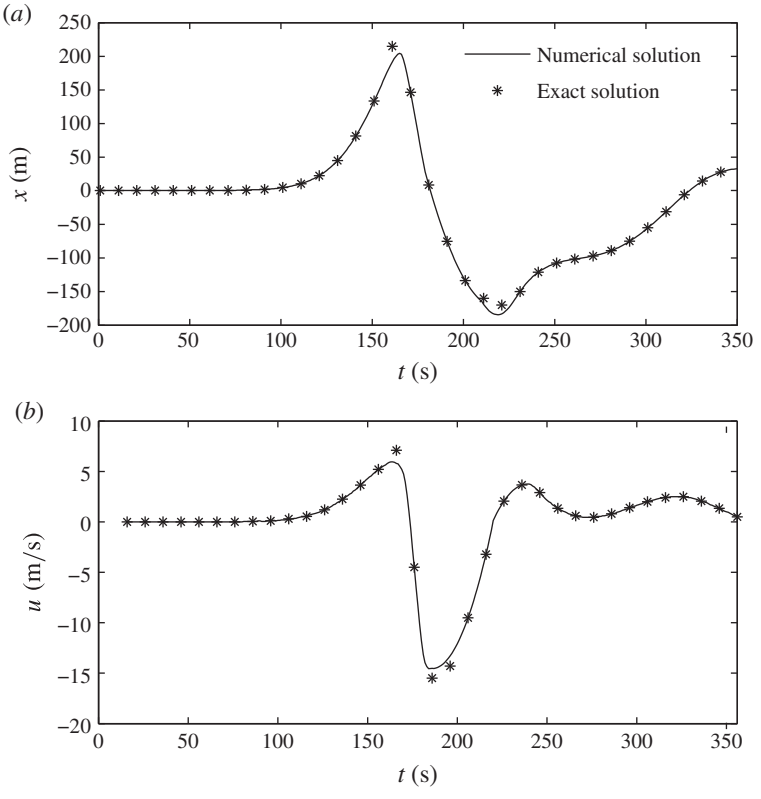

FIGURE 13. (*a*) The position and (*b*) the velocity of the wave front at different times.

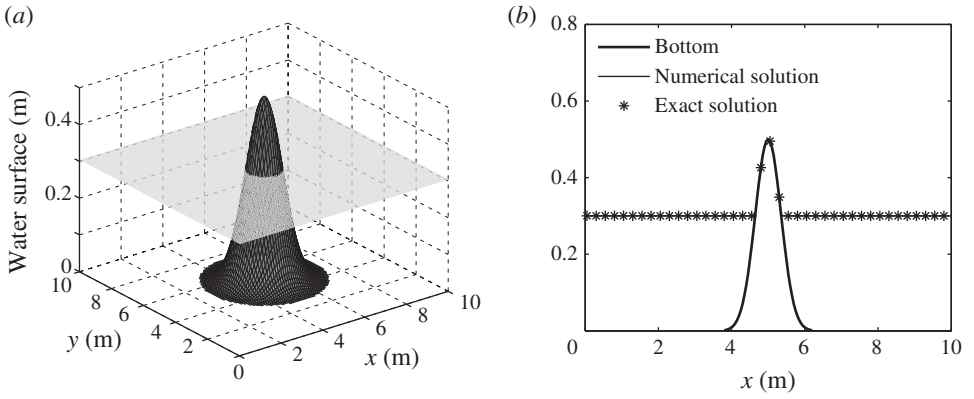

FIGURE 14. (*a*) A three-dimensional view of the water surface and the bed configuration; and (*b*) the water surface profile along the x direction for $y = 5$ after the simulation time reaches 50 s.

the movement of the wave front in terms of time series of its position and velocity, demonstrating a good agreement over the whole period, despite the fact that the maximum run-down and the corresponding velocity are slightly underestimated.

4.5. *A 2D stationary case with wet–dry boundaries*

In this numerical test, a simple case of still water over a variable bottom with a wet–dry boundary is investigated. A numerical scheme is considered to be well balanced if it can reproduce an exact solution to a stationary case in an uneven bed, which is referred to as the $\mathscr{N}$ property (Zhou 2004). This is a desirable basic test for a numerical scheme. To confirm that the proposed model satisfies this property, we consider a stationary case in 2D terrain consisting of an obstacle in the centre, which is defined by

$$z_b(x) = 0.5\mathrm{e}^{-4(r-5)^2}, \tag{4.11}$$

where $r = \sqrt{x^2 + y^2}$ on a 10 m $\times$ 10 m basin. The initial water level has been taken as 0.3 m in the basin. The simulation has been run for 50 s on 200×200 lattices. As expected, the use of the proposed wet–dry treatment generates no spurious solution at the wet–dry boundary and the water surface exactly preserves the stationary state (see figure 14).

4.6. *A 2D long-wave resonance in a parabolic basin*

A long-wave resonance driven by gravity in a parabolic basin provides a useful numerical test for the verification of a 2D shallow-water model for forecasting wetting–drying processes. Thacker (1981) described an analytical solution for such a case based on the NLSW equations. The free-surface displacement is given by

$$\eta(r, t) = h_0 \left(\frac{(1 - A^2)^{0.5}}{1 - A\cos(\omega t)} - 1 - \frac{r^2}{a^2} \left(\frac{1 - A^2}{(1 - A\cos(\omega t))^2} - 1 \right) \right) \tag{4.12}$$

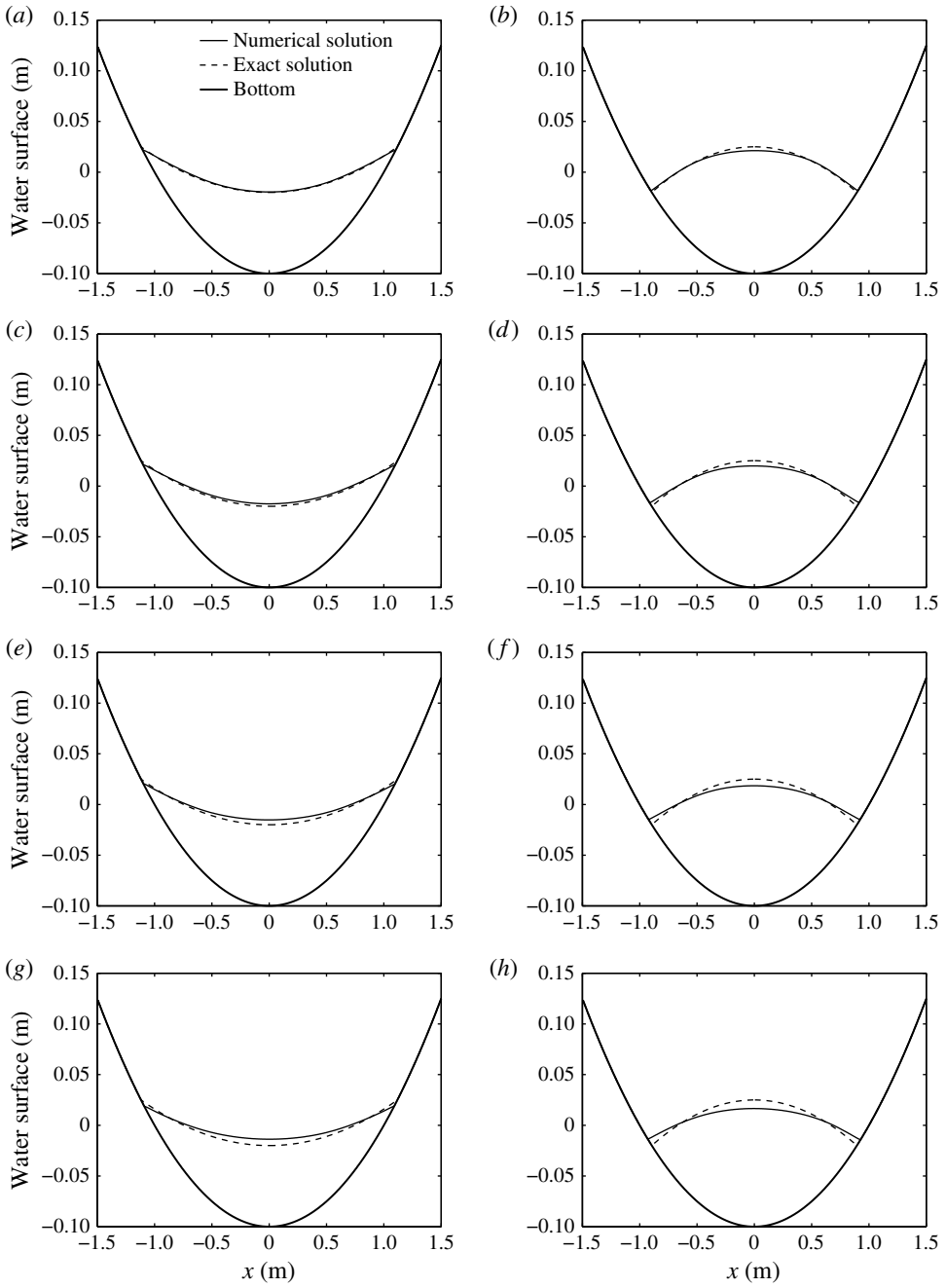

FIGURE 15. Comparisons of the water surfaces at different times: (*a*) $t = 0.5T$; (*b*) $t = T$; (*c*) $t = 1.5T$; (*d*) $t = 2T$; (*e*) $t = 2.5T$; (*f*) $t = 3T$; (*g*) $t = 3.5T$; (*h*) $t = 4T$.

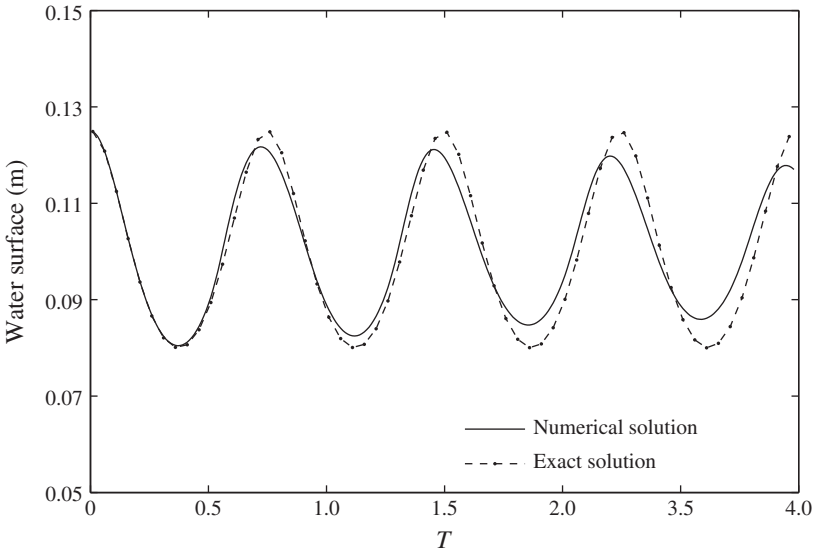

FIGURE 16. Water depth at the centre point.

and the bottom is defined as

$$z_b(r) = -h_0\left(1 - \frac{r^2}{a^2}\right), \tag{4.13}$$

in which

$$A = \frac{a^4 - r_0^4}{a^4 + r_0^4}, \quad \omega = \frac{1}{a}\sqrt{8gh_0}, \tag{4.14}$$

where h_0 is the water depth at the centre of the basin, r is the distance from the centre point and r_0 is the distance from the centre point to the point at the shoreline initially. In addition, a, r_0 and h_0 are set to 1, 0.8 m and 0.1 m, respectively, which are similar to those used by Marche *et al.* (2007). Through a grid convergence test, little difference in the numerical results can be found when the space step is changed from 0.005 to 0.01 m, and then the numerical model uses a 600×600 lattice on a 3 m $\times$ 3 m basin for study in detail. The relaxation time τ and the time step Δt are set to 0.62 and 0.001 s. As shown in figure 15, the overall agreements are good and wetting–drying processes for up to four cycles of oscillation period (T) have been successfully reproduced. Although the numerical results slightly deviate from the analytical solution as time increases, the error grows slowly, with the root-mean-square error over the whole period ($4T$) being about 0.5 % (see figure 16). Finally, figure 17 shows the three-dimensional views of the water surfaces at times $2T$ and $2.5T$, respectively.

4.7. *A 2D solitary wave run up on a conical island*

As a final test of the two-dimensional wetting and drying scheme, the solitary wave run up onto a conical island is simulated, which was studied experimentally

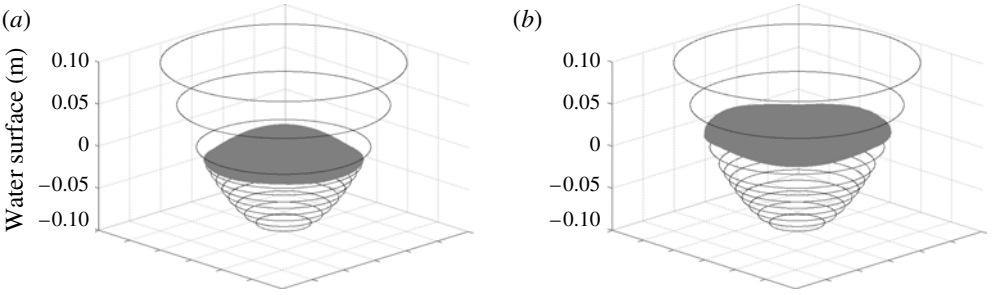

FIGURE 17. Three-dimensional views of the water surface: (*a*) $t = 2T$; (*b*) $t = 2.5T$.

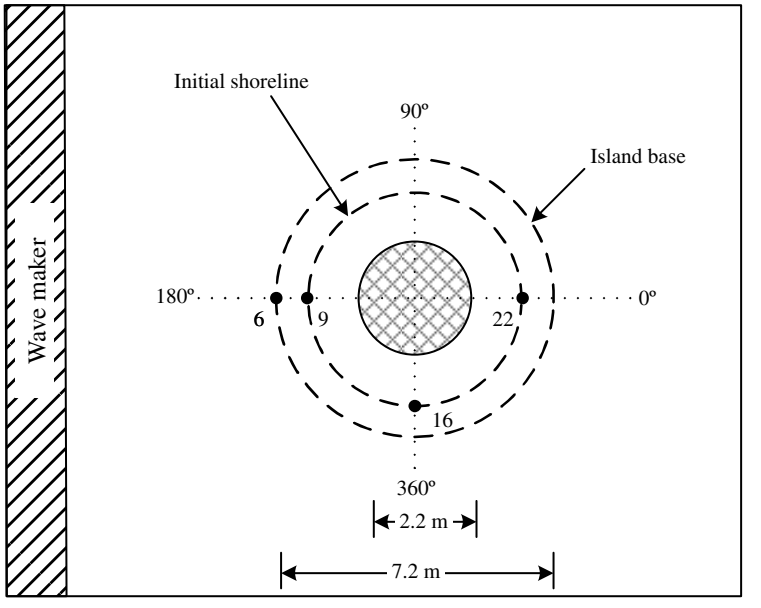

FIGURE 18. (Colour online) Conical island layout showing the gauge locations (black dots).

by Briggs *et al.* (1995) and Liu *et al.* (1995). A schematic diagram of the conical island and the locations of four gauges are plotted in figure 18, where a wave maker is placed at the left boundary and the two dashed circles are island base and initial shoreline. The island has 0.625 m height and 1/4 side slope. The diameters of the base and crest are 7.2 m and 2.2 m, respectively. The experimental results of $h_0 = 0.32$ m and $H/h_0 = 0.045$, 0.096 and 0.18 are used to validate the scheme. The computational domain consists of 250×300 lattices with $\Delta x = \Delta y = 0.1$ m. The time step $\Delta t = 0.01$ s and $\tau = 0.9$ are used.

The maximum run-up levels around the island have been validated against the experimental data and plotted in figure 19 for all three cases. The time series of the water surface displacement at four gauges are compared and presented in figures 20–22. As seen from these figures, the lead wave height and shape are well predicted, which are comparable to the results by Lynett *et al.* (2002) and Bradford & Sanders

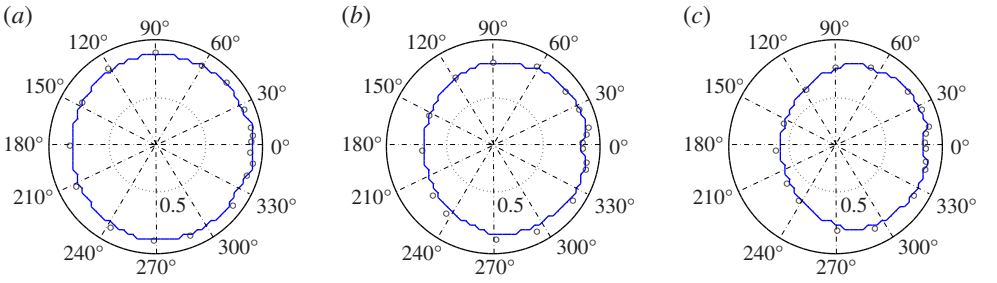

FIGURE 19. (Colour online) A bird's eye view of the maximum wave run-up around the conical island, with comparisons between the numerical results in lines and the measured data in dots: (*a*) $H/h_0 = 0.045$; (*b*) $H/h_0 = 0.096$; (*c*) $H/h_0 = 0.018$.

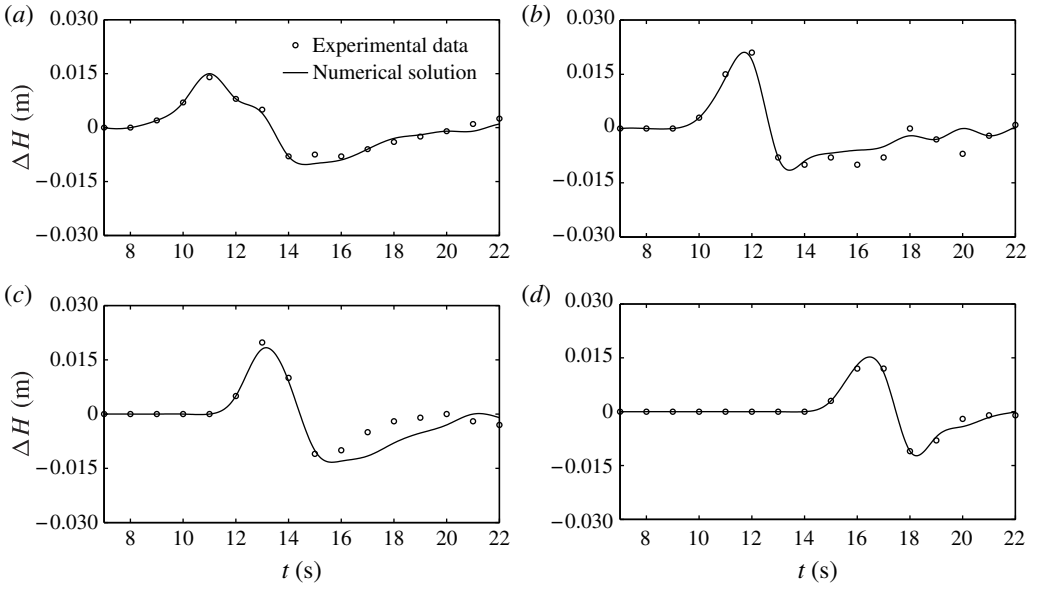

FIGURE 20. Comparisons of the water surface displacement for $H/h_0 = 0.045$ at various gauges: (*a*) gauge 6; (*b*) gauge 9; (*c*) gauge 16; (*d*) gauge 22.

(2002) using finite difference and finite volume methods, respectively. However, the secondary depression wave and the following perturbations of the surface are not accurately simulated compared with those presented by Hubbard & Dodd (2002) using a finite volume model with adaptive mesh refinement. This deviation is probably due to the fact that wave absorbers were placed at the boundaries in order to reduce wave reflection in the experiment, which is not taken into account in the present numerical simulations. Finally, the three-dimensional views of the water surface around the conical island have been shown in figure 23.

5. Conclusions

An approach to simulating wetting–drying processes in shallow-water flows is developed using the lattice Boltzmann method (LBM). The proposed scheme is derived from the theory of the LBM by linking the non-equilibrium particle

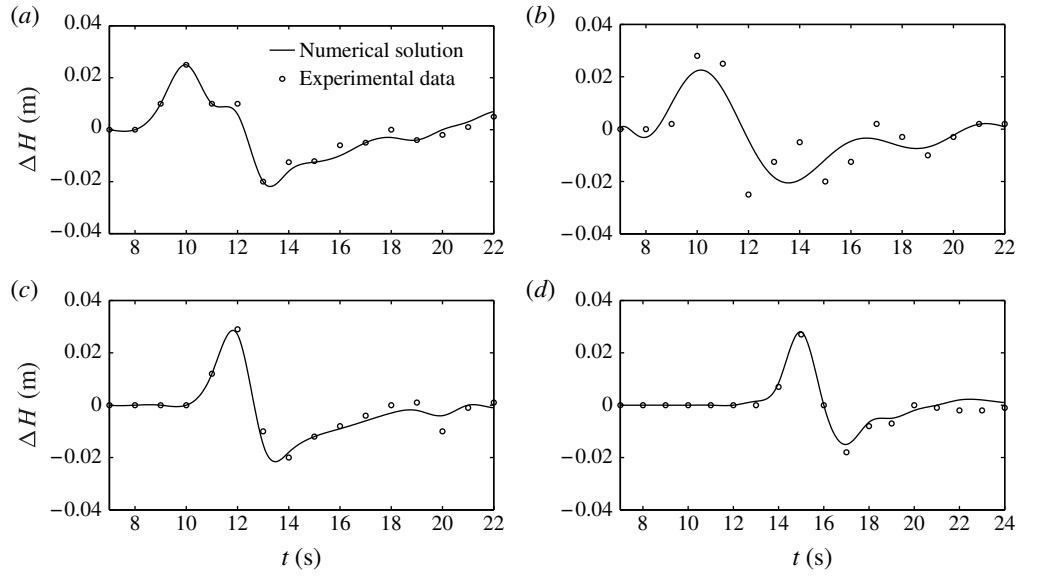

FIGURE 21. Comparisons of the water surface displacement for $H/h_0 = 0.096$ at various gauges: (*a*) gauge 6; (*b*) gauge 9; (*c*) gauge 16; (*d*) gauge 22.

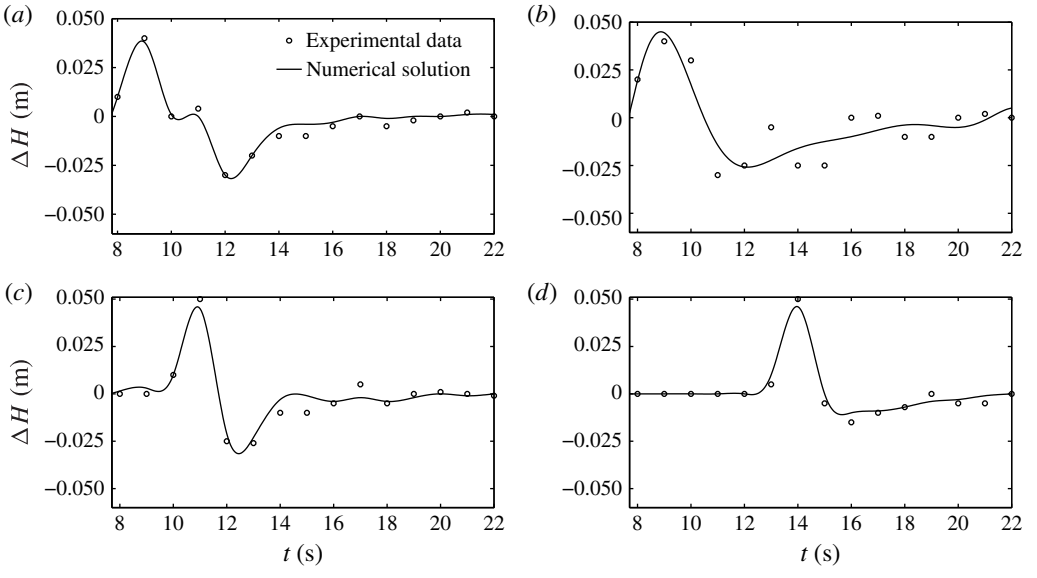

FIGURE 22. Comparisons of the water surface displacement for $H/h_0 = 0.18$ at various gauges: (*a*) gauge 6; (*b*) gauge 9; (*c*) gauge 16; (*d*) gauge 22.

distribution function of dry cells to those of their neighbouring wet cells, retaining the advantages of the LBM. This consequently yields a consistent incorporation of an external force into the scheme with the LBM, which ensures the correct simulation of the wet–dry phenomenon. The numerical results indicate that the scheme is able

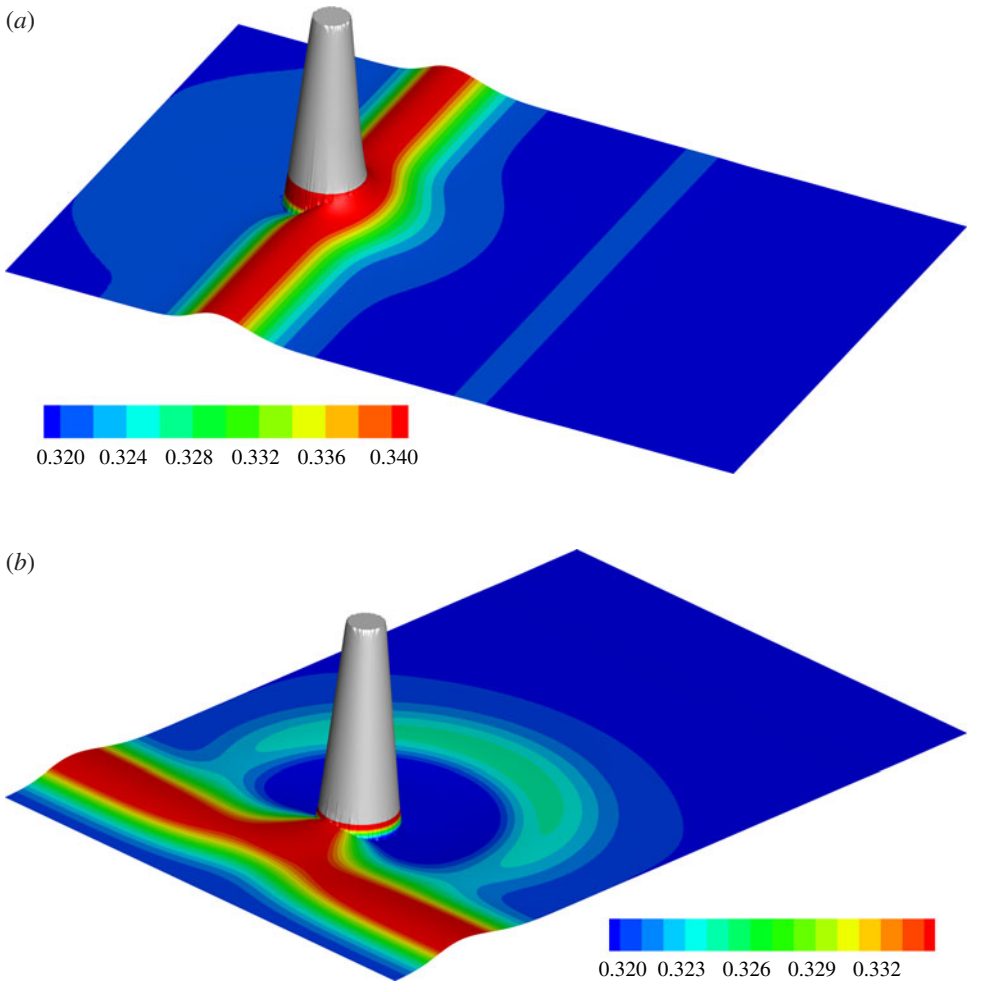

FIGURE 23. (Colour online) Three-dimensional views of the water surfaces around the conical island (water depth is shown in colour): (*a*) $t = 10$ s; (*b*) $t = 14$ s.

to predict different wetting–drying fronts over various bed configurations with bed frictions in good agreements with analytical solutions, other numerical results and experimental data. As additional forces can be correctly included in a straightforward way, the method will be attractive for modelling general complex wetting–drying processes occurring in practical shallow-water flows.

Acknowledgements

The financial support of the National Basic Research Program of China (973) (2011CB403304), the National Natural Science Foundation of China (51379001) and the National Key Technology Research and Development Program (2011BAC12B02) are gratefully acknowledged.

REFERENCES

BHATNAGAR, P., GROSS, E. P. & KROOK, M. K. 1954 A model for collision processes in gases: I. Small amplitude processes in charged and neutral one-component system. *Phys. Rev.* A **94**, 511–525.

BRADFORD, S. F. & SANDERS, B. F. 2002 Finite-volume model for shallow-water flooding of arbitrary topography. *J. Hydraul. Eng. ASCE* **128**, 289–298.

BRIGGS, M. J., SYNOLAKIS, C. E., HARKINS, G. S. & GREEN, D. R. 1995 Laboratory experiments of tsunami runup on a circular island. *Pure Appl. Geophys.* **144**, 569–593.

BRUFAU, P., VÁZQUEZ-CENDÓN, M. E. & GARCÍA-NAVARRO, P. 2002 A numerical model for the flooding and drying of irregular domains. *Int. J. Numer. Methods Fluids* **39**, 247–275.

CARRIER, G. F., WU, T. T. & YEH, H. 2003 Tsunami run-up and draw-down on a plane beach. *J. Fluid Mech.* **475**, 79–99.

CHEN, H., GOLDHIRSCH, I. & ORSZAG, S. 2008 Discrete rotational symmetry, moment isotropy, and higher order lattice Boltzmann models. *J. Sci. Comput.* **34**, 87–112.

DELIS, A. I., KAZOLEA, M. & KAMPANIS, N. A. 2008 A robust high-resolution finite volume scheme for the simulation of long waves over complex domains. *Int. J. Numer. Methods Fluids* **56**, 419–452.

DELLAR, P. 2002 Non-hydrodynamic modes and a priori construction of shallow water lattice Boltzmann equations. *Phys. Rev.* E **65**, 036309.

FRANDSEN, J. B. 2008 A simple LBE wave runup model. *Prog. Comput. Fluid Dyn.* **8**, 222–232.

GALLARDO, J. M., PARÉS, C. & CASTRO, M. 2007 On a well-balanced high-order finite volume scheme for shallow water equations with topography and dry areas. *J. Comput. Phys.* **227**, 574–601.

GEORGE, D. L. 2008 Augmented Riemann solvers for the shallow water equations over variable topography with steady states and inundation. *J. Comput. Phys.* **227**, 3089–3113.

HENICHE, M., SECRETAN, Y., BOUDREAU, P. & LECLERC, M. 2000 A two-dimensional finite element drying–wetting shallow water model for rivers and estuaries. *Adv. Water Resources* **23**, 359–372.

HIBBERD, S. & PEREGRINE, D. H. 1979 Surf and run-up on a beach: a uniform bore. *J. Fluid Mech.* **95**, 323–345.

HUBBARD, M. E. & DODD, N. 2002 A 2d numerical model of wave run-up and overtopping. *Coast. Eng.* **47**, 1–26.

JUNK, M., KLAR, A. & LUO, L.-S. 2005 Asymptotic analysis of the lattice Boltzmann equation. *J. Comput. Phys.* **210**, 676–704.

KÂNOĞLU, U. & SYNOLAKIS, C. E. 1998 Long wave runup on piecewise linear topographies. *J. Fluid Mech.* **374**, 1–28.

KENNEDY, A. B., CHEN, Q., KIRBY, J. T. & DALRYMPLE, R. A. 2000 Boussinesq modeling of wave transformation, breaking and runup. *J. Waterway Port Coast. Ocean Eng.* **126**, 39–47.

LECLERC, M., BELLEMARE, J.-F., DUMAS, G. & DHATT, G. 1990 A finite element model of Estuarian and river flows with moving boundaries. *Adv. Water Resources* **13**, 158–168.

LEVEQUE, R. J. & GEORGE, D. L. 2008 High-resolution finite volume methods for the shallow water equations with bathymetry and dry states. In *Advanced Numerical Models for Simulating Tsunami Waves and Runup* (ed. P. Liu, H. Yeh & C. Synolakis), Advances in Coastal and Ocean Engineering, vol. 10, pp. 43–73. World Scientific.

LI, Y. & RAICHLEN, F. 2002 Non-breaking and breaking solitary wave run-up. *J. Fluid Mech.* **456**, 295–318.

LIU, P. L.-F., CHO, Y.-S., BRIGGS, M.J., KÂNOĞLU, U. & SYNOLAKIS, C. E. 1995 Runup of solitary waves on a circular island. *J. Fluid Mech.* **302**, 259–285.

LIU, H., ZHOU, J. G. & BURROWS, R. 2010 Lattice Boltzmann simulations of the transient shallow water flows. *Adv. Water Resources* **33**, 387–396.

LIU, H., ZHOU, J. G. & BURROWS, R. 2012 Inlet and outlet boundary conditions for the lattice-Boltzmann modelling of shallow water flows. *Prog. Comput. Fluid Dyn.* **12**, 11–18.

LYNETT, P. J., WU, T.-R. & LIU, P. L.-F. 2002 Modeling wave runup with depth-integrated equations. *Coast. Eng.* **46**, 89–107.

MADSEN, P. A., SØRENSEN, O. & SCHÄFFER, H. A. 1997 Surf zone dynamics simulated by a Boussinesq type model. Part I. Model description and cross-shore motion of regular waves. *Coast. Eng.* **32**, 255–287.

MAHDAVI, A. & TALEBBEYDOKHTI, N. 2009 Modeling of non-breaking and breaking solitary wave run-up using FORCE-MUSCL scheme. *J. Hydraul. Res.* **47**, 476–485.

MARCHE, F., BONNETON, P., FABRIE, P. & SEGUIN, N. 2007 Evaluation of well-balanced bore-capturing schemes for 2D wetting and drying processes. *Int. J. Numer. Methods Fluids* **53**, 867–894.

ROGERS, B., FUJIHARA, M. & BORTHWICK, A. G. L. 2001 Adaptive *Q*-tree Godunov-type scheme for shallow water equations. *Int. J. Numer. Methods Fluids* **35**, 247–280.

SALMON, R. 1999 The lattice Boltzmann method as a basis for ocean circulation modeling. *J. Mar. Res.* **57**, 503–535.

SAMPSON, J., EASTON, A. & SINGH, M. 2006 Moving boundary shallow water flow above parabolic bottom topography. *ANZIAM J.* **47**, C373–C387.

SHAFIAI, S. H. 2011 Lattice Boltzmann method for simulating shallow free surface flows involving wetting and drying. PhD Thesis, University of Liverpool.

SYNOLAKIS, C. E. 1986 The runup of long waves. PhD Thesis, California Institute of Technology, Pasadena.

SYNOLAKIS, C. E. 1987 The runup of solitary waves. *J. Fluid Mech.* **185**, 523–545.

THACKER, W. C. 1981 Some exact solutions to the nonlinear shallow-water wave equations. *J. Fluid Mech.* **107**, 499–508.

TITOV, V. V. & SYNOLAKIS, C. E. 1995 Modeling of breaking and nonbreaking long-wave evolution and runup using VTCS-2. *J. Waterway Port Coast. Ocean Eng.* **121**, 308–316.

ZELT, J. A. 1991 The run-up of nonbreaking and breaking solitary waves. *Coast. Eng.* **15**, 205–246.

ZHOU, J. G. 2002 A lattice Boltzmann model for the shallow water equations with turbulence modeling. *Int. J. Mod. Phys.* C **13**, 1135–1150.

ZHOU, J. G. 2004 *Lattice Boltzmann Methods for Shallow Water Flows*. Springer.

ZHOU, J. G. 2011 Enhancement of the LABSWE for shallow water flows. *J. Comput. Phys.* **230**, 394–401.